



High-performance OLEDs based on 4,5-diaza-9,9'-spirobifluorene ligated rhenium(I) complex with enhanced steric hindrance

Xiao Li ^{a,*}, Hai-Jun Chi ^a, Gong-Hao Lu ^a, Guo-Yong Xiao ^a, Yan Dong ^a, Dong-Yu Zhang ^{b,*}, Zhi-Qiang Zhang ^a, Zhi-Zhi Hu ^a

^aSchool of Chemical Engineering, University of Science and Technology Liaoning (USTL), Anshan 114051, People's Republic of China

^bSuzhou Institute of Nano-Tech and Nano-Bionics (SINANO), Chinese Academy of Sciences, Suzhou 215123, People's Republic of China

ARTICLE INFO

Article history:

Received 17 May 2012

Received in revised form 18 September 2012

Accepted 23 September 2012

Available online 6 October 2012

Keywords:

4,5-Diaza-9,9'-spirobifluorene

Rhenium complex

Phosphorescence

OLEDs

ABSTRACT

Highly efficient and emitter concentration insensitive phosphorescent electroluminescent devices based on a novel rhenium(I) [Re(I)] complex, i.e., (4,5-diaza-9,9'-spirobifluorene)Re(CO)₃Br (Re-DSBF), were established. Non-doped device based on Re-DSBF as emitter exhibited outstanding performances with the peak luminance of 8531 cd m⁻² and maximum current efficiency of 16.8 cd A⁻¹, which were the highest reported to date for non-doped phosphorescent electroluminescent devices based on Re(I) emitters. Such excellent performances are closely related to the steric hindrance, large Stokes shift, and short luminescent lifetime of Re-DSBF complex. The luminescent mechanisms of those devices were also investigated.

© 2012 Elsevier B.V. All rights reserved.

1. Introduction

Organic light-emitting diodes (OLEDs) possess latent application prospects in eco-friendly flat-panel displays and energy-saving solid-state lightings owing to rapid progress in material design and device fabrication [1–3]. Of the light-emitting organic materials available, phosphorescent materials have attracted extensive attention in recent years owing to their promising advantages of achieving a maximum internal quantum efficiency of nearly 100% [4–6]. In view of the distinguished qualities of rhenium(I) [Re(I)] complexes which possess such as photophysical, photochemical, excited state redox properties and with the aim of further exploring novel phosphorescent materials, many researchers pay considerable attention to this field [7–10]. For example, Mu et al. [11] recently reported

efficient devices based on [2-(4'-diphenylaminophenyl)-1,10-phenanthroline]Re(CO)₃Cl with a maximum current efficiency of 12.2 cd A⁻¹ and a peak brightness of 7308 cd m⁻² by a solution process, which represented the best values reported for electrophosphorescent devices based on solution processable Re(I) complexes, but these values were still much lower than those of Re(I)-doped devices fabricated by vacuum deposition methods [12,13]. Very recently, Mauro et al. [14] reported phosphorescent OLEDs with outstanding external quantum efficiency of ca. 10% using binuclear Re(I) complexes as dopants, which was the highest reported for phosphorescent OLEDs with Re(I)-based phosphors up to now.

Due to the poor carrier mobility and luminescence self-quenching of the intrinsic phosphorescent dopants, high-performance phosphorescent OLEDs are usually fabricated by doping the emitters into a charge-transporting host matrix in a rather low and narrow concentration range. However, the complicated low-doped process which usually requires a precise control of dopant ratio limits the practical applications in mass production. Therefore, it is of significant importance and interest for OLEDs applica-

* Corresponding authors. Tel.: +86 412 5929627; fax: +86 412 5929637.

E-mail addresses: aslxiiao@yahoo.com.cn (X. Li), dyzhang2012@yahoo.com.cn (D.-Y. Zhang).

tions to explore new phosphorescent materials that can serve as efficient high-doped or non-doped emitters.

It is well-known that 4,5-diaza-9,9'-spirobifluorene (DSBF), which has two almost mutually perpendicular π -system linked by a common tetrahedral atom and rigid backbone, exhibits high electron affinity [15]. Wong et al. [16] reported a DSBF derivative as efficient electron injection/transport material and blue emitter in OLEDs. Then, Wu et al. [17] reported highly efficient single-layered solid-state light-emitting electrochemical cells based on iridium (III) complexes containing DSBF ligand which could greatly enhance the steric hindrance of iridium (III) complexes and reduce self-quenching of luminescence. Lately, Du et al. [18] reported a DSBF functionalized europium (III) complex with efficient photo- and electroluminescent properties.

Hinted by aforementioned those, highly efficient and emitter concentration insensitive phosphorescent OLEDs based on a novel Re(I) emitter, i.e., (4,5-diaza-9,9'-spirobifluorene)Re(CO)₃Br (Re-DSBF), were achieved. More importantly, the non-doped device based on Re-DSBF emitter showed prominent performances with the peak luminance of 8531 cd m⁻² and maximum current efficiency of 16.8 cd A⁻¹.

2. Experimental details

2.1. Materials and instruments

Commercially available reagents were used without further purification unless otherwise stated. Re(CO)₅Br was available from Alfa Aesar. Solvents were dried by standard procedures prior to use. NMR spectra were recorded on a Bruker AC 500 spectrometer. Chemical shifts were reported in ppm down field from tetramethylsilane (TMS) with the solvent resonance as the internal standard. Elemental analysis was performed on Vario EL III CHNS instrument. FTIR spectra were recorded with samples as KBr pellets using WQF 200 FTIR spectrophotometer. Thermogravimetric analysis (TGA) was undertaken under nitrogen atmosphere at a heating rate of 10 °C min⁻¹ on a Perkin-Elmer Diamond TG-DTA 6300 thermal analyzer. UV-vis absorption spectrum was obtained on a Perkin-Elmer Lambda 900 spectrophotometer. Photoluminescent (PL) spectra were measured on a Perkin-Elmer LS 55 fluorescence spectrophotometer. PL quantum yield of the Re(I) complex was measured according to the reference's method [7]. The luminescent lifetimes of the Re(I) complex were detected by a system equipped with a TDS 3052 digital phosphor oscilloscope pulsed Nd:YAG laser with a Third-Harmonic-Generator 355 nm output. Cyclic voltammetry experiments were conducted using a CHI832B electrochemical analyzer with a scan rate of 200 mV s⁻¹. All measurements were carried out at room temperature (RT).

2.2. Material synthesis

2.2.1. Synthesis of DSBF

DSBF was synthesized according to the reference method [16]. Magnesium (0.24 g, 10 mmol) and a little iodine

were added into the flask under nitrogen atmosphere, then the mixture solvents of THF (0.5 mL) and 1,2-dichloroethane (0.1 mL) were added. Subsequently, the system was heated and stirred for about 20 min to active the magnesium. Then 2-bromobiphenyl (1.9 mL, 11 mmol) in 9.5 mL THF was added dropwise into this mixture. The reaction was stopped until the magnesium disappeared completely. Under refluxing, the flask containing above resulting 2-biphenylmagnesium bromide was added into 4,5-diazafluorene-9-one (0.91 g, 5 mmol) in 25 mL THF. The mixture was refluxed for about 12 h, and then quenched with water after cooling to ambient temperature and extracted with CHCl₃. The combined organic solution was dried with MgSO₄ and concentrated by rotary evaporation. The resulting crude solid was washed with *n*-hexane and dried to give 5-biphenyl-2-yl-5H-cyclopenta [2,1-b;3,4-b']dipyridin-5-ol as a brown solid (1.232 g, yield: 73%). The resulting intermediate of 5-biphenyl-2-yl-5H-cyclopenta [2,1-b;3,4-b']dipyridin-5-ol, 100 mL acetic acid and 1.5 mL sulfuric acid were refluxed for about 24 h under nitrogen atmosphere. The reaction was quenched with cold water after cooling to RT and neutralized with saturated NaOH (aq) to basic, then extracted with CHCl₃ and dried with MgSO₄. The combined organic solution was concentrated by rotary evaporation, washed with *n*-hexane and dried to give DSBF as light brown solid. Yield: 51%. MS (APCI): *m/z* 319.2 [M + H⁺]. ¹H NMR (500 MHz, CDCl₃, TMS): δ 8.7 (s, 2 H), 7.87 (d, *J* = 7.63 Hz, 2 H), 7.41 (dd, *J* = 7.445 Hz, 2 H), 7.14–7.12 (m, 6 H), 6.73 (d, *J* = 7.585 Hz, 2 H); IR (KBr, cm⁻¹): 3026, 1402, 1167, 752.

2.2.2. Synthesis of Re-DSBF

DSBF (0.33 g, 1.1 mmol) and Re(CO)₅Br (0.41 g, 1 mmol) were refluxed in 100 mL of toluene for 3 h under nitrogen atmosphere. After the mixture was cooled to RT, the solvent was removed and the resulting yellow solid was purified by silica-gel column chromatography with acetic ether and petroleum ether as mobile phase. Yield: 76%. ¹H NMR (500 MHz, CD₂Cl₂, TMS): δ 8.68–8.66 (m, 2 H), 7.87 (d, *J* = 7.695 Hz, 1 H), 7.82 (d, *J* = 7.635 Hz, 1 H), 7.43 (dd, *J* = 7.565 Hz, 1 H), 7.37 (dd, *J* = 7.558 Hz, 1 H), 7.32–7.28 (m, 4 H), 7.18 (dd, *J* = 7.60 Hz, 1 H), 7.08 (d, *J* = 7.55 Hz, 1 H), 6.89 (d, *J* = 7.625 Hz, 1 H), 6.68 (d, *J* = 7.635 Hz, 1 H); ¹³C NMR (125 MHz, CD₂Cl₂, TMS): 161.705, 150.669, 143.003, 142.441, 141.590, 141.494, 134.063, 129.561, 129.324, 128.780, 128.381, 127.214, 124.045, 123.986, 120.964, 120.782; IR (KBr, cm⁻¹): 2025, 1927, 1886, 1283, 1230; Elemental analysis for C₂₆H₁₇BrN₂O₃Re. Calcd: C, 46.50; H, 2.55; N, 4.17; Found: C 46.52, H 2.53, N 4.19.

2.3. Device fabrication and EL measurements

OLEDs were fabricated through vacuum deposition of the materials at about 1 × 10⁻⁶ Torr onto ITO-coated glass substrates with a sheet resistance of 25 Ω sq⁻¹. The ITO-coated substrates were routinely cleaned by ultrasonic treatment in solvents and then cleaned by exposure to a UV-ozone ambient. All organic layers were deposited in succession without breaking vacuum. The devices were prepared with the conventional structures of ITO/m-MTDATA

(10 nm)/NPB (20 nm)/CBP: *x*% Re-DSBF (30 nm)/Bphen (10 nm)/Alq₃ (20 nm)/LiF (1 nm)/Al (120 nm), in which m-MTDATA {4,4',4''-tris[3-methylphenyl(phenyl)amino]triphenyl-amine}, NPB {4,4'-bis[N-(1-naphthyl)-N-phenyl-amino]biphenyl}, CBP (4,4'-N,N'-dicarbazolebiphenyl), Bphen (4,7-diphenyl-1,10-phenanthroline), and Alq₃ [tris(8-hydroxyquinoline)aluminum] were used as hole injection layer, hole transporting layer, host, exciton blocking layer and electron transporting layer, respectively, and LiF/Al as the composite cathode. Deposition rates and thicknesses of the layers were monitored *in situ* using oscillating quartz monitors. Thermal deposition rates for organic materials, LiF, and Al were ~ 1 , ~ 1 , and $\sim 10 \text{ \AA s}^{-1}$, respectively. EL spectra were measured by a PR655 spectra scan spectrometer. The luminance–current–voltage (*I*–*I*–*V*) characteristics were recorded simultaneously with the measurement of EL spectra by combining the spectrometer with a Keithley 2400 source meter. All measurements were carried out at RT under ambient conditions.

3. Results and discussion

3.1. Synthesis and characterization

The synthetic routes of Re-DSBF complex were showed in Scheme 1. The synthesis of spiroconfigured ligand DSBF involved three steps including spiro oxidation, nucleophilic addition and electrophilic substitution reactions using 1,10-phenanthroline as starting material [16]. Among the synthesis processes, it should be specially pointed out that the preparation for Grignard reagent based on 2-bromobiphenyl required strict condition control because of large steric hindrance of 2-bromobiphenyl. Then, Re-DSBF was smoothly obtained by direct complexation of DSBF with Re(CO)₅Br in refluxing toluene for good isolated yield. The molecular structure was fully characterized by ¹H NMR, ¹³C NMR, and element analysis, respectively. The molecular structure of Re-DSBF was further confirmed by IR spectra. Three C=O stretching vibration bands were observed in IR spectrum, characteristic of monomeric

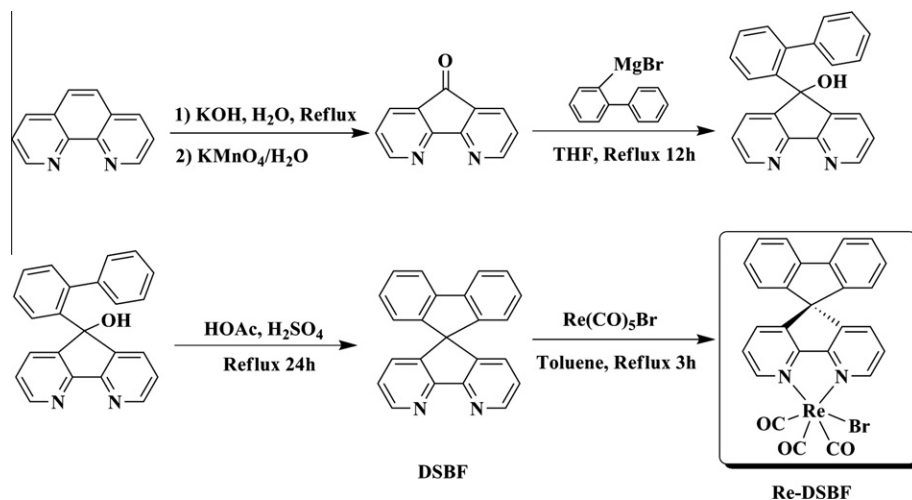
pseudooctahedral *fac*-Re(CO)₃⁺ [19]. All evidences indicated that the resulting Re(I) complex conformed to the proposed structure.

The thermal stability of the complex was carried out by TGA under a nitrogen stream. Re-DSBF was thermally stable up to ca. 330 °C corresponding to 5% weight loss, as determined in Fig. 1, which was beneficial to the long-term stability of OLEDs fabricated from the material.

3.2. Photophysical properties

Fig. 2 showed the UV absorption and PL spectra of Re-DSBF in dilute dichloromethane solution and solid PL spectrum of 25% Re-DSBF doped in CBP film. Absorption spectrum of Re-DSBF was very similar to those of analogous Re(I) tricarbonyl complexes [20], and the assignments had been made accordingly. By comparison to the absorption of the free ligand DSBF, the absorption bands of Re-DSBF located at ca. 270 and 305 nm could be assigned to spin-allowed ¹ π – π^* DSBF-centered electronic transitions. The moderately intense, poorly distinguished absorption bands extending into the visible region from ca. 350 to 500 nm were tentatively assigned to an admixture of metal-to-ligand charge transfer states, $d\pi(\text{Re}) \rightarrow \pi^*(\text{DSBF})$ (¹MLCT and ³MLCT). The PL spectrum of Re-DSBF in dichloromethane showed a green emission with a maximum emission centered at 530 nm, which had been assigned as MLCT-based luminescence, typical of this type of complex [21]. From solid PL spectrum (25% Re-DSBF doped in CBP), strong emission at 545 nm including weak emission at about 420 nm which should be attributed to the emission of CBP can be detected, indicating that efficient energy transfer occurs between CBP and Re-DSBF.

The PL quantum yield of Re-DSBF in chloroform solution was measured to be 0.15 using quinine sulfate ($\phi = 0.546$) as a calibration standard, which was much higher than those of previously reported Re(I) complexes based on 4,5-diazafluorene derivatives [22]. The spiroconfigured DSBF ligand effectively enhanced the steric hindrance of Re(I) complex and reduced the self-quenching



Scheme 1. Synthetic routes of Re-DSBF complex.

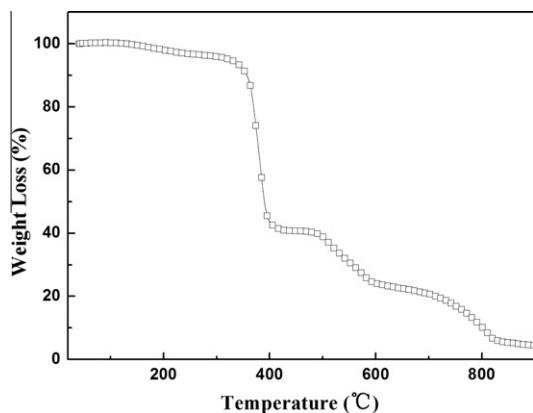


Fig. 1. TGA trace of Re-DSBF in N_2 atmosphere at a heating rate of $10^\circ C\ min^{-1}$.

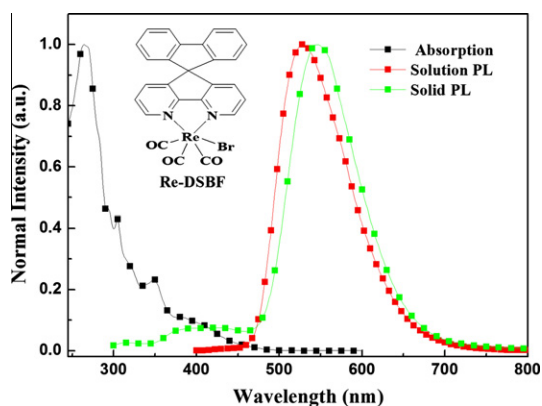


Fig. 2. UV absorption and PL spectra of Re-DSBF in dilute dichloromethane solution and solid PL spectrum of 25% Re-DSBF doped in CBP film.

effect, so PL measurement showed highly retained quantum yield.

As shown in Fig. 2, there was little overlap between the absorption and emission spectra of the Re(I) complex. The Stokes shift for Re-DSBF which was obtained between the maximum of the lowest energy absorption band and the maximum of the emission band was as large as about 180 nm. The large Stokes shift may be caused by significant structural differences between the ground state and excited state upon photo excitation. More importantly, such a large Stokes shift was especially valuable for light-emitting materials used in high doped or non-doped OLEDs since the absence of self-absorption would definitely facilitate efficient light emission.

It has been well recognized that phosphorescence lifetime has significant influence in triplet–triplet annihilation. The longer phosphorescence lifetime of a material increases the possibility of triplet–triplet annihilation it potentially has. A very short lifetime ($0.12\ \mu s$) of Re-DSBF in solid state powder was obtained owing to molecule–molecule interactions. Therefore, the short phosphorescence lifetime of Re-DSBF could efficiently suppress the phosphorescence self-quenching to exhibit high efficiency. In order to further

determine the intrinsic triplet-state lifetime (τ_0) of Re-DSBF, the lifetimes of Re-DSBF in degassed chloroform at different concentrations from 1.0×10^{-5} to $1.0 \times 10^{-3}\ mol\ L^{-1}$ were measured. The Stern–Volmer kinetics equation $\tau_0/\tau = 1 + k_q \cdot C$ could be used to depict the relationship of the measured lifetimes τ and Re-DSBF concentration C , where k_q was the quenching rate constant. τ_0 and k_q were calculated to be $0.5\ \mu s$ and $2.53 \times 10^8\ mol^{-1}\ s^{-1}$, respectively. The intrinsic lifetime τ_0 exhibited a slight change at different concentrations and k_q was below the diffusion-controlled limit of $\sim 10^{10}\ mol^{-1}\ s^{-1}$ [23]. This phenomenon further demonstrated that there existed weak concentration quenching in Re-DSBF solution.

3.3. Electrochemical properties

The electrochemical behavior of Re-DSBF was investigated by CV, which was shown in Fig. 3. The anodic waves are associated with a Re^I-based oxidation process (Re^I/Re^{II}), and the cathodic waves are associated with a ligand (L)-based reduction process ($[Re^I Br(CO)_3(L)]/[Re^I Br(CO)_3(L^-)]^-$) [24,25]. Re-DSBF shows irreversible anodic waves at $E_{1/2} = +1.53\ V$ with an onset oxidation potential of $+1.06\ V$. The energy level of the highest occupied molecular orbital (HOMO) is calculated from the onset oxidation (E_{onset}^{Ox}) with the formula $E_{HOMO} = -4.8 - E_{onset}^{Ox}$ ($-4.8\ V$ for saturated calomel electrode with respect to the zero vacuum level) to be $-5.86\ eV$ for Re-DSBF. The energy band gap of Re-DSBF obtained from the optical absorption spectrum is $2.68\ eV$, so the lowest unoccupied molecular orbital (LUMO) is determined to be $3.18\ eV$.

3.4. Density functional theory calculations on Re(I) complex

The ground state geometries and electronic structures of Re-DSBF were calculated according to density functional theory (DFT) calculations using the GAUSSIAN-03 software package (Gaussian, Inc.) at the B3LYP/LANL2DZ level since such investigations had been proven to be very helpful in understanding the photophysical properties of Re(I) complexes [26]. Therefore, it would be instructive to examine the HOMOs and the LUMOs of this complex.

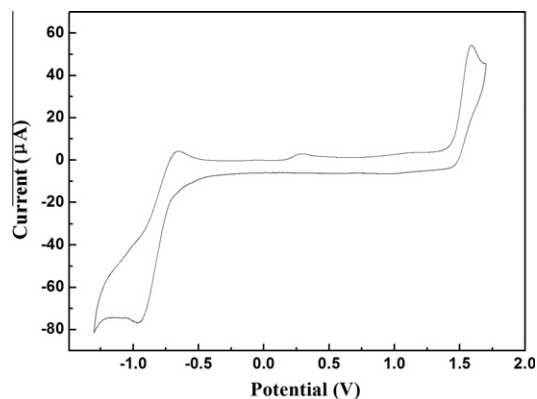


Fig. 3. Cyclic voltammograms of Re-DSBF measured in CH_2Cl_2 (vs. SCE) at a scan rate of $200\ mV\ s^{-1}$.

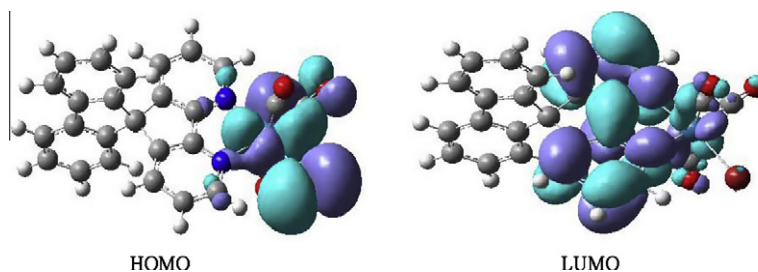


Fig. 4. Contour plots of HOMOs and LUMOs for Re-DSBF as determined by DFT calculations.

Table 1

EL performance parameters of different Re(I)-doped electrophosphorescent devices.

Device	$\lambda_{\text{max}}^{\text{a}}$ /nm	CIE (x,y) at 6 V	$L_{\text{max}}^{\text{b}}$ /cd m ⁻²	$\eta_{\text{L}}^{\text{c}}$ /cd A ⁻¹	$\eta_{\text{L}}^{\text{d}}$ /cd A ⁻¹
I	548	(0.363,0.591)	4840	5.4	4.0
II	548	(0.365,0.587)	7195	7.4	6.5
III	550	(0.370,0.572)	8990	12.1	8.9
IV	557	(0.395,0.576)	8531	16.8	8.5

^a Maximum emission wavelength.

^b Maximum luminance.

^c Maximum current efficiency.

^d Current efficiency at 100 mA cm⁻².

As could be seen from Fig. 4, the ground state geometries of Re-DSBF displayed a distorted octahedral configuration of ligand around the metal center. The calculated geometries of Re-DSBF showed that the biphenyl unit was significantly twisted against to the 4,5-diazafluorene core, resulting in a non-planar structure in Re-DSBF molecule. The geometrical characteristic could effectively suppress molecular packing. The HOMOs of Re-DSBF were mainly composed of the π orbitals of the carbonyl group, the bromine, and the d orbitals of Re cation which were in antibonding coordination with the axial bromine group and bonding with the three carbonyl groups. While the LUMOs of Re-DSBF were essentially π^* orbital localized on almost the whole 4,5-diazafluorene moiety with slim contributions from Re cation. These results also indicated that introduction of biphenyl unit in Re-DSBF hardly affected the HOMOs and LUMOs levels of Re-DSBF, and so its green emission was similar to that of our previously reported Re(I) complexes based on 4,5-diazafluorene derivatives [22]. Our calculated results were well in agreement with previous reports [26].

3.5. Electroluminescent properties

To investigate EL properties of Re-DSBF as emitter, four devices with a typical multi-layer configuration of ITO/m-MTDATA/NPB/CBP: $x\%$ Re-DSBF/Bphen/Alq₃/LiF/Al were fabricated. Devices I, II and III used Re-DSBF doped in CBP with different doping levels (8% in device I, 15% in II and 25% in III), while device IV utilized Re-DSBF as a non-doped emitter. Key EL parameters of devices I–IV were summarized in Table 1.

All devices exhibit yellowish-green emissions, which are insensitive to the applied voltages at the wide range of 3–16 V. The EL spectra of devices I–IV at the same

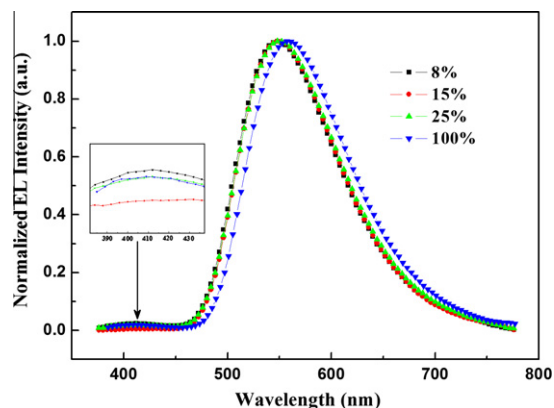


Fig. 5. EL spectra of devices I–IV at the voltage of 6 V.

voltage of 6 V are shown in Fig. 5. It can be found that EL spectra of devices I–IV consist of very weak emission bands at about 400–430 nm. The weak emissions in doped devices should originate from CBP, compared with solid PL spectrum of 25% Re-DSBF doped in CBP. The inconspicuous emissions from CBP support a model of charge trapping [27]. However, the weak emission at about 420 nm in non-doped device should be attributed to NPB emission. The maximum EL emissions of devices I, II and III are almost same, which appear at ca. 548 nm. The maximum emission of non-doped device IV appears at 557 nm, which is slightly red-shifted for about 10 nm probably owing to the stronger intermolecular interaction. Compared with PL spectrum in dichloromethane solution, a red shift of about 20 nm is observed in the EL spectra, which is frequently observed among light-emitting materials mainly because of the effect of the electrical field on the excited states.

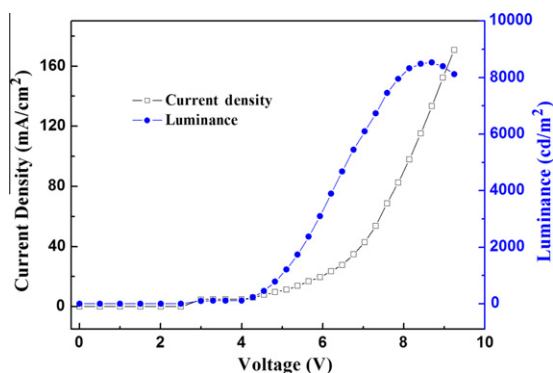


Fig. 6. L - I - V characteristic of non-doped device IV.

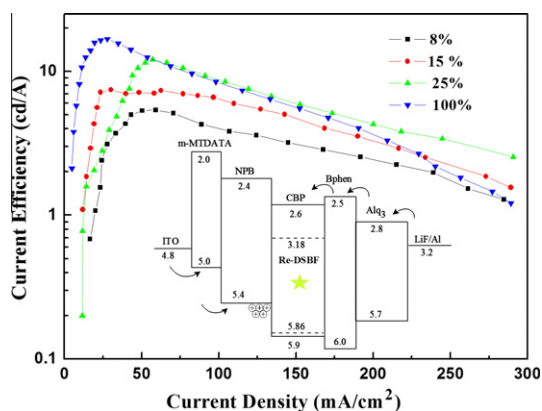


Fig. 7. Current efficiency-current density curves of devices I-IV. Inset: the proposed energy levels diagram.

The L - I - V characteristics of device IV are plotted in Fig. 6. The non-doped device exhibits a peak luminance of 8531 cd m^{-2} at 8.5 V, which is better than those of the most Re(I)-based OLEDs [12,13]. The turn-on voltage of the device is lower than 4 V. The device efficiency varies with the doping concentration of Re-DSBF, as shown in Fig. 7. Device IV shows the highest current efficiency of 16.8 cd A^{-1} at the current density of 28 mA cm^{-2} , which is the highest ever reported for non-doped phosphorescent OLEDs based on Re(I)-complex emitters and not far from those of the Re(I)-doped OLEDs [12–14]. The higher efficiency at high doping concentrations probably results from largely suppressed self-quenching of Re-DSBF. It is particularly interesting that the EL efficiency firstly increases at relatively low current density until it reaches a maximum value. This phenomenon could be elucidated as follows: at low current density, excess hole injection generates because of the much higher hole mobility of NPB ($\mu_h = 5.1 \times 10^{-4} \text{ cm}^2 \text{ V}^{-1} \text{ s}^{-1}$) than the electron mobility of Alq₃ ($\mu_e = 1.4 \times 10^{-6} \text{ cm}^2 \text{ V}^{-1} \text{ s}^{-1}$) [28,29], and consequently charge carrier balance is not well established. With increasing current density, the good electron-transporting ability of Re-DSBF could improve the charge balance, then resulting in gradually increasing efficiency.

In order to further evaluate electron-transporting behavior of Re-DSBF, electron-only single-carrier device

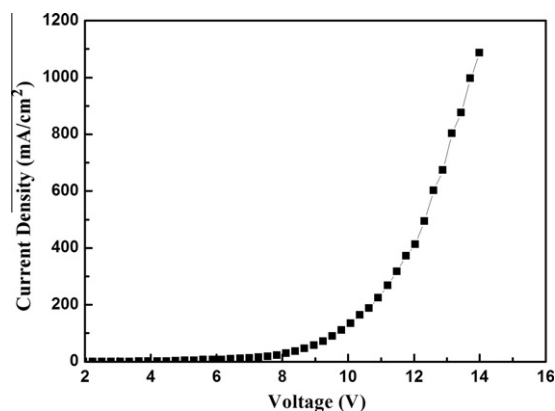


Fig. 8. Current density-voltage curve of electron-only single-carrier device with the structure of ITO/BCP/Re-DSBF/BCP/LiF/Al.

with the structure of ITO/BCP (10 nm)/Re-DSBF (30 nm)/BCP (10 nm)/LiF (1 nm)/Al) was fabricated. As shown in Fig. 8, current density is greatly increasing with voltage, demonstrating that Re-DSBF has superior electron-transporting ability.

As shown in inset of Fig. 7, there is 0.5 eV HOMO hole barrier at NPB/CBP interface, and the holes transferred from NPB will accumulate at the NPB/CBP interface. Those accumulated holes are in favor of electrons trapped on dopant. The device efficiency increases with the voltage, suggesting that carrier trapping plays a role in this work [30]. These results demonstrated that Re-DSBF is a very promising candidate for practical applications in OLEDs.

4. Conclusions

In conclusion, highly efficient phosphorescent OLEDs had been achieved by using a new emitter Re(I) complex with enhanced steric hindrance. In particularly, non-doped device based on this Re(I) complex exhibited the peak luminance of 8531 cd m^{-2} and the maximum efficiency of 16.8 cd A^{-1} , which were among the highest reported to date for non-doped OLEDs based on Re(I) complexes. Such excellent performances were probably attributed to the steric hindrance, large Stokes shift, and short luminescent lifetime of Re-DSBF complex. Those encouraging results imply that the phosphorescent transition metal complexes containing ligands with good electron-transporting property and superior steric hindrance are excellent candidates for highly efficient OLEDs in commercial production.

Acknowledgements

Authors gratefully acknowledge the supports from the National Natural Science Foundation of China (Grant No. 61204021), the Project from Department of education of Liaoning Province (Grant No. L2012094), Open Fund of Key Laboratory of Functional Materials, Colleges and Universities in Liaoning Province (Grant No. USTLKL 2012-02) and Research Project for Young Teachers of USTL (Grant No. 2010Y08).

References

- [1] Y. Sun, N.C. Giebink, H. Kanno, B. Ma, M.E. Thompson, S.R. Forrest, *Nature* 440 (2006) 908.
- [2] S. Reineke, F. Lindner, G. Schwartz, N. Seidler, K. Walzer, B. Lüssem, K. Leo, *Nature* 459 (2009) 234.
- [3] W.-Y. Wong, C.-L. Ho, *Coord. Chem. Rev.* 253 (2009) 1709.
- [4] Y. Chi, P.-T. Chou, *Chem. Soc. Rev.* 39 (2010) 638.
- [5] E. Holder, B.M.W. Langeveld, U.S. Schubert, *Adv. Mater.* 17 (2005) 1109.
- [6] G. Zhou, W.-Y. Wong, X. Yang, *Chem. Asian J.* 6 (2011) 1706.
- [7] K.Z. Wang, L. Huang, L.H. Gao, L.P. Jin, C.H. Huang, *Inorg. Chem.* 41 (2002) 3353.
- [8] Z.J. Si, J. Li, B. Li, F.F. Zhao, S.Y. Liu, W.L. Li, *Inorg. Chem.* 46 (2007) 6155.
- [9] X. Li, D.Y. Zhang, H.J. Chi, G.Y. Xiao, Y. Dong, S.H. Wu, Z.S. Su, Z.Q. Zhang, P. Lei, Z.Z. Hu, W.L. Li, *Appl. Phys. Lett.* 97 (2010) 263303.
- [10] N.J. Lundin, A.G. Blackman, K.C. Gordon, D.L. Officer, *Angew. Chem. Int. Ed.* 45 (2006) 2582.
- [11] X. Liu, H. Xia, W. Gao, Q. Wu, X. Fan, Y. Mu, C. Ma, *J. Mater. Chem.* 22 (2012) 3485.
- [12] C.B. Liu, J. Li, B. Li, Z.R. Hong, F.F. Zhao, S.Y. Liu, W.L. Li, *Appl. Phys. Lett.* 89 (2006) 243511.
- [13] X. Li, D.Y. Zhang, W.L. Li, B. Chu, L.L. Han, J.Z. Zhu, Z.S. Su, D.F. Bi, D. Wang, D.F. Yang, Y.R. Chen, *Appl. Phys. Lett.* 92 (2008) 083302.
- [14] M. Mauro, C.-H. Yang, C.-Y. Shin, M. Panigati, C.-H. Chang, G. D'Alfonso, L. De Cola, *Adv. Mater.* 24 (2012) 2054.
- [15] K. Ono, T. Yanase, M. Ohkita, K. Saito, Y. Matsushita, S. Naka, H. Okada, H. Onnagawa, *Chem. Lett.* 33 (2004) 276.
- [16] K.-T. Wong, R.-T. Chen, F.-C. Fang, C.-C. Wu, Y.-T. Lin, *Org. Lett.* 7 (2005) 1979.
- [17] H.-C. Su, F.-C. Fang, T.-Y. Hwu, H.-H. Hsieh, H.-F. Chen, G.-H. Lee, S.-M. Peng, K.-T. Wong, C.-C. Wu, *Adv. Funct. Mater.* 17 (2007) 1019.
- [18] S.M. Wang, J.Y. Zhang, Y.H. Hou, C.X. Du, Y.J. Wu, *J. Mater. Chem.* 21 (2011) 7559.
- [19] M.J. Paterson, M.A. Robb, L. Blancafort, A.D. DeBellis, *J. Phys. Chem. A* 109 (2005) 7527.
- [20] M.S. Wrighton, D.L. Morse, *J. Am. Chem. Soc.* 96 (1974) 998.
- [21] J.K. Hino, L. Della Ciana, W.J. Dressick, B.P. Sullivan, *Inorg. Chem.* 31 (1992) 1072.
- [22] X. Li, D. Zhang, W. Li, B. Chu, L. Han, T. Li, Z. Su, J. Zhu, S. Wu, Y. Chen, P. Lei, Z. Hu, Z. Zhang, *Synthetic Met.* 159 (2009) 1340.
- [23] Z. Murtaza, A.P. Zipp, L.A. Worl, D. Graff, W.E. Jones Jr., W. Doug Bates, T.J. Meyer, *J. Am. Chem. Soc.* 113 (1991) 5113.
- [24] G.J. Stor, F. Hartl, J.W.M. Van Outersterp, D.J. Stufkens, *Organometallics* 14 (1995) 1115.
- [25] S. Berger, A. Klein, W. Kaim, J. Fiedler, *Inorg. Chem.* 37 (1998) 5664.
- [26] L. Yang, A.-M. Ren, J.-K. Feng, X.-J. Liu, Y.-G. Ma, M. Zhang, X.-D. Liu, J.-C. Shen, H.-X. Zhang, *J. Phys. Chem. A* 108 (2004) 6797.
- [27] N.C. Erickson, R.J. Holmes, *Appl. Phys. Lett.* 97 (2010) 083308.
- [28] B. Chen, C.-S. Lee, S.-T. Lee, P. Webb, Y.-C. Chan, W. Gambling, H. Tian, W. Zhu, *Jpn. J. Appl. Phys.* 39 (2000) 1190.
- [29] R.G. Kepler, P.M. Beeson, S.J. Jacobs, R.A. Anderson, M.B. Sinclair, V.S. Valencia, P.A. Cahill, *Appl. Phys. Lett.* 66 (1995) 3618.
- [30] P.W.M. Blom, M.J.M. de Jong, J.J.M. Vleggaar, *Appl. Phys. Lett.* 68 (1996) 3308.